β^- energy Analysis in ^{15}P: Application to Betavolatics : A theoretical Analysis

S. R. Mirfayzi

School of Physics and Astronomy University of Birmingham Birmingham B15 2TT United Kingdom

E-mail: srm105@bham.ac.uk

Abstract. Using radioactive nuclei for electricity generation in Microelectromechanical Systems (MEMS) is important research as needs for longer life batteries increase. There are many applications developed in recent years, however there are limitations still to overcome before a final product can be produced. One of the important issue is the low power output. This research addresses this issue with a new method in fabrication for powering MEMS sensors. We have proposed to fabricate ^{63}Ni nano-particle β^-source in a glassy phosphorous type sphere which creates scintillation and phosphorescent photons. The micro-spheres will be doped in our semiconductor. Since ^{63}Ni is a pure β^- emitter, in this report the energy loss dE/dx of β^- in our scintillation material (phosphorus ^{15}P) is modelled using C++ coding with GEANT4 and furthermore the particle distributions in two different source geometries (circular and square structure) is studied using Finite Element Analysis (FEA). We have shown the $63Ni$ β energy spectrum absorption in $15P$, where upto energy range 28keV had nearly 100% efficiency. The optimum thickness therefore achieved was $800\mu m$.

1. Introduction

Betavolatics are direct charge batteries where charges on β particles directly drive a current. In this research a new type of Betavolatics are proposed, where a ^{63}Ni (source) will be fabricated inside phosphorus (^{15}P) spherical containers, and (^{15}P) elements are then doped in silicon lattice. The energy lost from β particles to the absorber (^{15}P) is then derived into the solar arrays for final conversion essentially the phosphorous-solar cell system acts as an impedance matching device converting a high voltage, low current (e.g 17keV single electron) into a useful power source (e.g 2V, 100mA. It is convenient to split the energy loss process into two different categories on the base of their scattering properties into elastic and inelastic process. In elastic scattering the target remains intact and in inelastic scattering the particle loses its kinetic energies to the target and causes other internal process. The process of inelastic scattering analysed using two different methods, Bethe and Gyrzinski. The Bethe theory is looking at the loss by Born approximation to calculate the cross section, where Gyrzinski attempts to obtain the cross section by looking at the inner-shells ionisation. The Inelastic Mean Free Path (IMFP) is also obtained and reported. The particle flow distributions at two geometries and radiation absorption in ^{15}P are modelled using Neumann-Dirichlet boundary condition.

2. Theoretical Calculations

Environmental factors and material surroundings are always defined using boundary conditions. Enforcing boundary condition on flux requires an intensive numerical treatment. In this model the boundary conditions are defined using Dirichlet equation. By using Dirichlet we are able to impose the Laplace equation (our transport equation) to the system domain. Figure 1 demonstrates Dirichlet boundary conditions for circle and square geometry for an incoming flux.

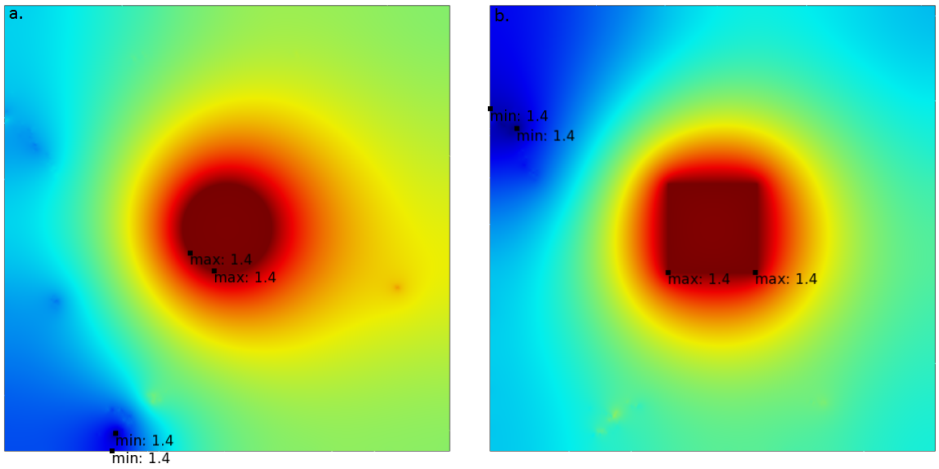

Figure 1. Particles flow on the surface of the ^{63}Ni source. At figure 1a enter the surface from circle structure where in figure 1b enters the surface from a square structure. The unit on the source is dimensionless.

As shown the flux in figure 1a enters the surface from circle structure where in figure 1b enters the surface from a square structure. To understand the behaviour first it is more convenient to have the numerical Laplace for both cases.

$$\Delta = \frac{\delta^2 U}{\delta x^2} + \frac{\delta U}{\delta y^2} \tag{1}$$

Circular Laplace has true Dirichlet boundary everywhere between $0 < r < 1$ and $U = r^m sin(m\theta)$ [1]. As given in figure 1 the local minima and maxima in the domain is defined on the boundary (this is one of the Laplace properties as they tend to be harmonic, the value 1.4 is a arbitrary threshold that is defined to study the Lagrange function). In the square structure we have Dirichlet boundary conditions everywhere except $y = 1$ (also $0 < x < 1$). Thus $U(x, y) = \Sigma_{n=1}^{\infty} C_n sinh(n\pi y) sin(n\pi x)$ and $C_n = 2\int_0^1 f(x) sin(n\pi x) dx / sinh(n\pi)$.
Now that Laplace equation is defined we need to numerically define the flux and multiply the two values. Thus we will have:

$$\bigtriangledown .(-c \bigtriangledown u - \alpha u + \gamma) \tag{2}$$

Here α is the velocity term, γ is the source term and equation 2 is called flux vector. c can be also indirectly calculated for an anisotropic material. The flux term can be also calculated using continuity equation. Hence in more general form (where the material convection, absorption and conservative flux convection is set zero), our problem can be simplified and written as:

$$\frac{\delta u}{\delta t} + \bigtriangledown((\bigtriangledown \rho + \frac{I_r}{r})I_z) \tag{3}$$

Equation 3 is in computational domain (ω), thus we need to satisfy all conditions in boundary domain. This is called Neumann-Dirichlet where the boundary will be transformed from ω to $d\omega$ (from computational boundary to domain boundary). This transformation is also described as domain decomposition preconditioner [2]. Thus the partial differential equation is given by $\bigtriangledown^2 u + u = 0$ where $\bigtriangledown$ donated as Laplacian therefore we will have:

$$\frac{du}{dn}(x) = \bigtriangledown^2 u(x).n(x) \tag{4}$$

Where n refers to a normal vector, thus we can rewrite the Eq. 2 as

$$n.(c \bigtriangledown u + \alpha u - \gamma) = g - h_N^t \tag{5}$$

where g and h_N^t donate the boundary source term and the Lagrange multiplier factor. h_N^t is needed in a mixed field situation as it corresponds to local maxima and minima. In some respect h_N^t can also refers to the velocity [3]. Hence we can rewrite the equation 3 as:

$$n.(\bigtriangledown(\rho + \frac{I_r}{r})I_z) = g - h_N^T \tag{6}$$

This called Neumann generalised boundary condition (in general form the h_N^T should be zero. Often h_N^T is replaced by Dirichlet condition and that equals to $\underline{h}u$). Now that our Boundary Conditions on particle flow are defined, the energy loss properties are also need to be statistically tackled. Model I is looking at the Bethe Theory in which the behaviour of each atom is studied in terms of transmission from their initial states to final states and the Model II is based on the Gryzinski's model looking at the energy loss of atoms due to their inner shell electron excitations. As the elastic scattering involves interactions of electrons with atomic nuclei and since the atomic nuclei is thousands times more massive than an electron, the energy transfer that involves elastic scattering is often insignificant, however this energy can reach up to ten thousands of electronvolt for a small fraction of electrons. The general term to determine the scattering is given by differential cross section of an incident electron over a solid angle Ω:

$$d\sigma/d\Omega = \left|f^2\right| \tag{7}$$

Where f is the atomic scattering factor which is given in function of scattering angle . The differential cross section in elastic form is represented by:

$$\frac{4}{a_0^2 q^4} \left|f(q)\right|^2 = \frac{4}{a_0^2 q^2} \left|Z - f_x(q))\right|^2 \tag{8}$$

where a_0 is the Bohr radius $0.529E^{-10}$ m, Z is the atomic density and the $f_x(q)$ is the scattering factor for an incident electrons. This usually is set to zero in classical and wave mechanical theory. By having the relativistic factor γ equal to $1 + E_0/(m_0 c^2)$ thus we can have:

$$\frac{d\sigma}{d\Omega} = \frac{4\gamma^2 Z^2}{a_0^2 q^4} \left\{1 - \frac{1}{(1 + (q r_0)^2)^2}\right\} \tag{9}$$

where the $q = 2k_0 sin(\frac{\theta}{2})$ is the momentum transfer; and k is the wave vector of the electron

before and after the scattering event.

$$\frac{d\sigma_i}{d\Omega} = \frac{4\gamma^2 Z}{a_0^2 q^4} \tag{10}$$

Where r_0 is the screening radius given by Wenz formula [6] in which shows the nuclear potential attenuation as function of r distance is given by:

$$\phi\,(r) = [Ze/4\pi\varepsilon_0 r]\, exp\left(\frac{-r}{r_0}\right) \tag{11}$$

The q in form of inelastic will be slightly modified as it depends on the initial and final scattering angle. Therefore in inelastic scattering it equals to $q^2 = k_0^2(\theta^2 - \theta_E^2)$. Here $k = \frac{2\pi}{\lambda}$ is the characteristic angle corresponding to average energy loss. By having the latter in an stationary state the $\frac{4\gamma^2 Z}{a_0^2 q^2}$ in Eq.11 represents the Rutherford scattering cross section in an elastic form [7]. Using Eq.10 and Eq.11, figure 2 is generated to demonstrate the inelastic cross section as function of angle.

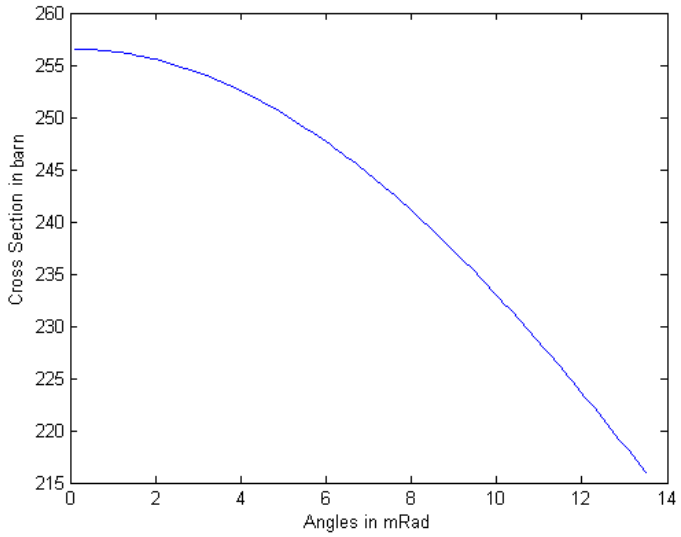

Figure 2. The Angular Dependence of Differential Cross Section of 200eV in ^{15}P. The inelastic scattering cross section decreases as the scattering angle increases

As Figure 2 demonstrates the inelastic scattering cross section decreases as the scattering angle increases. This figure reveals that most of the scattering happens to be in range of $\theta_E < \theta < \theta_0$. This roughly proportional to $1/\theta^2$. This shows higher probability of scattering in the forward direction. Gyrzinski's approach enabled the calculations to measure the energy loss due to the excitation. Gryzinskis stopping power simply can be calculated by replacing the [9] calculation (Eq.12) by Bethe. Hence the direct simulation of individual excitation specifically in the valance band will be more feasible. Since there are a limited number of electrons available in the inner shell, the inelastic stopping power is calculated by taking away the portion of energy lost to the valance band. Thus we have:

$$(\frac{dE}{dx}) = (\frac{dE}{dx})_{total} - \Sigma_i(\frac{dE}{dx})_i \tag{12}$$

Here the first term is the total energy loss and the second term represent the energy lost to valence electrons. Thus i shows the number valance electron which the equation is solved for. Now the Gyrzinski Stopping power can be calculated from (for derivation see [9]):

$$(\frac{dE}{dx}) = n_i \pi e^4 \frac{1}{E} (\frac{E - E_i}{E + E_i})^{1.5} [ln \frac{E}{E_i} + \frac{4}{3} ln[2.7 + \frac{E}{E_i} - 1]]^{0.5} \tag{13}$$

Where n_i is the number of electrons, E_i is the binding energy and E is the incident energy. The second term demonstrates the relativistic factor and the factor 2.7 corresponds to atomic ionization potential. Thus the formula for excitation energy is given by:

$$\frac{d\sigma_i}{d(\Delta E)} = n_i \pi e^4 \frac{1}{(\Delta E)^3} \frac{E_i}{E} (\frac{E}{E + E_i})^{1.5} (1 - \frac{\Delta E}{E})^{E_i + \Delta E} \times [\frac{\Delta E}{E_i} (1 - \frac{E_i}{E}) + \frac{4}{3} ln[2.7 + (\frac{E - \Delta E}{E_i})^{0.5}]] \tag{14}$$

ΔE is the energy loss. Now cross section can be calculated from:

$$\sigma_i = n_i \pi e^4 \frac{1}{E_i^2} \frac{E_i}{E} (\frac{E - E_i}{E + E_i})^{1.5} [1 + \frac{2}{3} (1 - \frac{E_i}{2E}) \times ln[2.7 + (\frac{E}{E_i} - 1)^{0.5}]] \tag{15}$$

Girzinskys formula provides an easy approach to calculate the relative energy loss. The simulation is done at $200eV$ incident electron interacting with three inner shell electrons of ^{15}P. Using equation 14 and 15 the magnitude of the excitation energy lost was calculated, and that was +69.6eV, hence the $\frac{dE}{dx}$ due to inelastic scattering is 130.4eV per 200eV.
So far the loss due to excitation is determined using Gyrzinski approach thus we required to verify the loss by inelastic scattering in more details using Bethe formula. The Bethe theory can be used to evaluate the behaviour of each atomic electrons in terms of transition from initial state to final state. This process will be angular dependent. [10] has approached this problem using first Born approximation, therefore differential cross section can be determined by:

$$d\sigma_n = (2\pi)^{-2} M^2 \hbar^{-4} (k^{'}/k) \int exp(iK.r) u_n * (r_1, ..., r_z) \times V u_0(r_1, ..., r_z) dr_1 ... dr_z dr)|^2 dw, \tag{16}$$

where M is the reduced mass of colliding system, r is the position of particle relative to the centre of atom, $\hbar k$ is the momentum of particle before the collision and $\hbar$ is the momentum after the collision, u is the eigenfunction of r_j coordinates whose the total number is Z. Now we can have the Eq.2.10 in angular form:

$$\frac{d\sigma_n}{d\Omega} = (\frac{m_0}{2\pi\hbar^2})| \int V(r) \psi_0 \psi_n^* exp(iq.r) d\tau|^2 \tag{17}$$

Here the initial states and final states are ψ_0 and ψ_n^*. k_0 and K_1 are the wave-vectors and $V(r)$ is the potential energy required by each collision. The $V(r)$ is required due to existence of Coulomb force and it is required by Bethe theory. It can be calculated using:

$$V(r) = \frac{Ze^2}{4\pi\varepsilon_0 r} - \frac{1}{4\pi\varepsilon_0} \sum_{j=1}^{Z} \frac{e^2}{|r - r_j|} \tag{18}$$

Where the first term represents the Rutherford scattering and $|\varepsilon_n(q)|^2$ is the dynamical structure

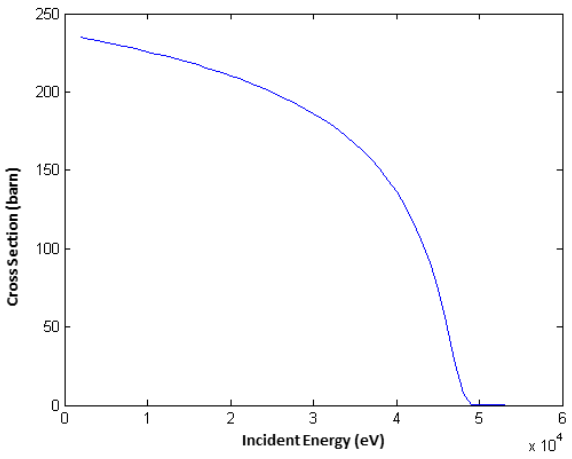

Figure 3. Gyrzinski's differential Cross Section. The differential cross section (in barn) is calculated for Gyrzinski (Eq. 14) cross section. Only done for low energy calculation, with higher energy considered another rising peak should expected.

factor. The dynamical structure factor is closely related to the generalised oscillator strength [10]. And is calculated using Rydberg energy ($13.61eV$) and transition energy. Figure 3 demonstrates the differential cross section calculated with Gyrzinski's equation(Eq.14). It is clear that the inner shell electrons contribute relatively little to the cross section. One of the major role in ionization depends on a process called elastic ionization. To determine the energy loss due to elastic scattering the Eq.9 should to be modified. As mentioned before the elastic scattering is caused by interaction of incident electron beams with electrostatic field of nuclei. By transferring enough energy to the rest mass projectile atom, it will be scattered from the shell after the collision and causes the atom to be ionized. In this case the Eq.9 is simply rewritten as:

$$\frac{d\sigma}{d\Omega} = \frac{4\gamma^2 Z^2}{a_0^2 q^4} \tag{19}$$

Having electrons scattered elastically makes the second term in Eq.9 zero. This is due to the estimation for the screening radius which is defined in Eq.11. Thus by using Eq.11 one more time we can define the differential cross as function scattering angle:

$$\frac{d\sigma}{d\Omega} = \frac{4\gamma^2 Z^2}{a_0^2(q^2 + r_0^{-2})} \approx \frac{4\gamma^2 Z^2}{a_0^2 k_0^4} \frac{1}{(\theta^2 + \theta_0^2)^2} \tag{20}$$

Where $\theta_0 = (k_0 r_0)^{-1}$ is the characteristic angle. The r_0 can be redefined using Thomas-Fermi approximation ($r_0 = a_0 Z^{-1/3}$). For an ionized atom the $\frac{d\sigma}{dE}$ increases with decrease in the characteristic angles. The elastic scattering energy transfer can be also given by:

$$E = E_{max} sin^2(\theta/2) = E_{max}(1 - cos\theta)/2 = E_{max}(1 - cos\theta)/2 \tag{21}$$

Where E_{max} is the energy transfer at maximum angle and is calculated from [11] as:

$$E_{max}^2 = 2E_0(E_0 + 2M_0c^2) \tag{22}$$

The differential cross section is at its minimum at central impact $\theta = 0$ and increases by increase in the angle.
Now that the loss due to ionization and excitation is measure the IMFP can be calculated.The model describing IMFP is based on a theoretical approach to the transport of primary electron beams on the surface, thus a relationship between signal intensity and concentration of given elements in an elastic and inelastic deferential cross section is required. This could be a complex function as the accurate data from elastic and inelastic cross section is not obtainable. Hence the computational functions are usually solved by looking into continuous slowing down approximation (CSDA) in which an electron energy along the trajectory is assumed to be a function of length. To tackle this problem the excitation function for a charged particle is defined by its dielectric function. As demonstrated by [12]:

$$\frac{d^2\sigma}{d(\Delta E)dq} = \frac{me^2}{\pi\hbar^2 NE} Im(\frac{-1}{\varepsilon(\omega,q)})\frac{1}{q} \tag{23}$$

Where N is number density of the atom and E is the energy of incident beam, (ΔE) is the energy loss and $Im(\frac{-1}{\varepsilon(\omega,q)})$ is the dielectric function. Dielectric function can be reduced to a more generalised form of Lindhard type dielectric function [13] and [14]. In This model the IMFP is calculated based on [15] and [16]approach:

$$\lambda = \frac{E}{E_p^2[\beta ln(0.191\rho^{-0.5}E) - (1.97 - 0.91(N_v\rho/M)/E) + ((53.4 - 20.8(N_v\rho/M)/E^2)]} \tag{24}$$

Here the ρ is the material density and E_g is the band gap energy, M is the atomic weight, $\beta = -0.1 + 0.944(E_p^2 + E_g^2)^{-0.5} + 0.069\rho^{0.1})$, $E_P = 28.8(N_v\rho/M)^{0.5}$ is the free electron plasmon energy, and N_v is the number of valence electron per atom.

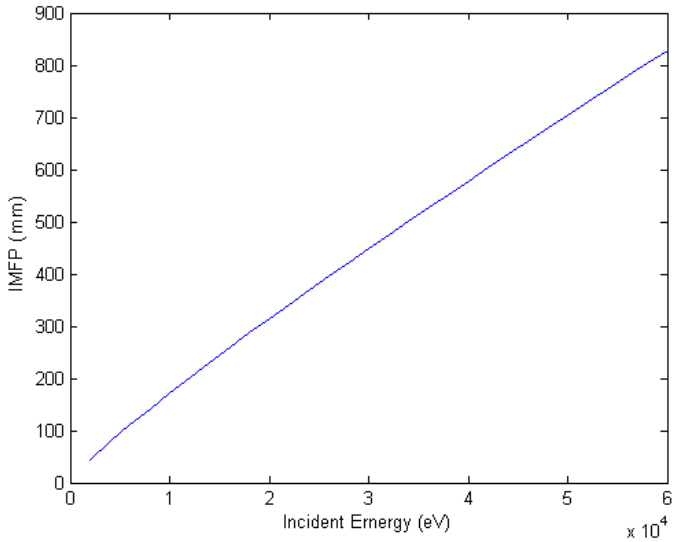

Figure 4. Inelastic Mean Free Path in ^{15}P. As the incident energy increases the IMFP also increases.

Figure 4 demonstrates use of Eq. 2.19 for ^{15}P in our case. In this case the N_v is set to 5, $M = 30.97$, $E_q = 3eV$ and $\rho = 1.88g/cm^3$. These are the value which are typical for our material (data from NIST library).

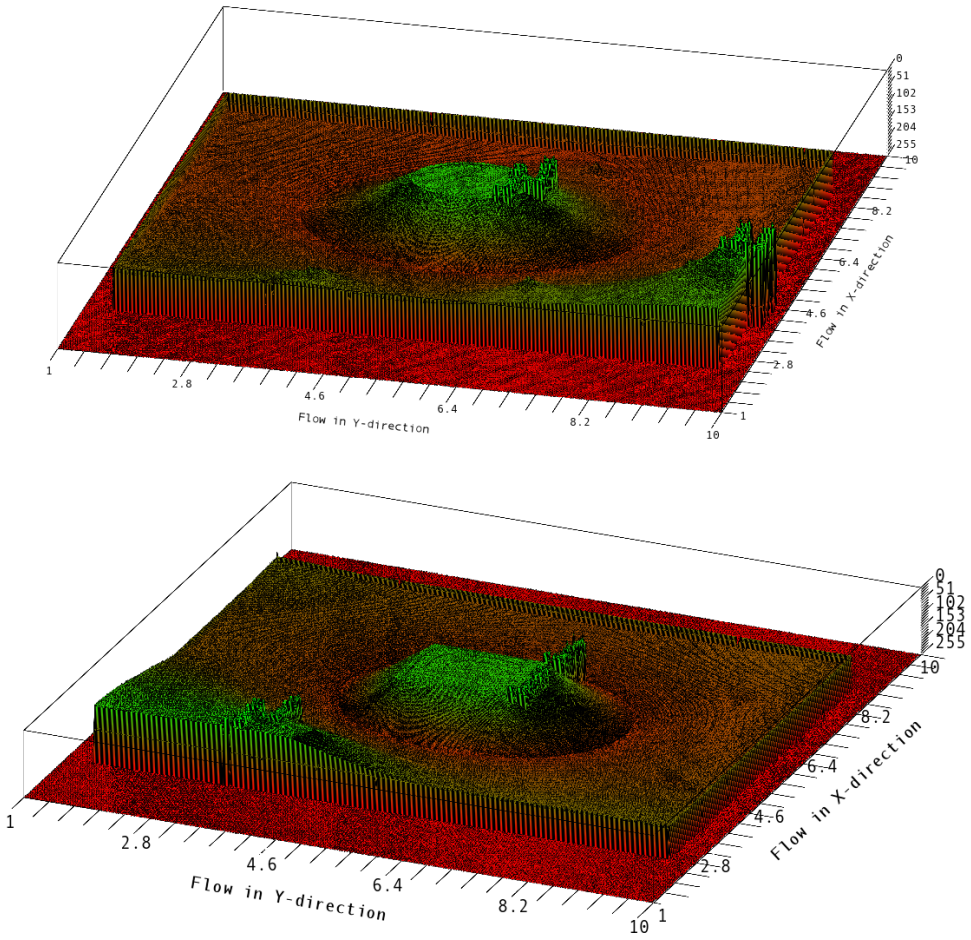

Figure 5. The Particle Distribution in ^{63}Ni. The distribution in circular geometry is lower in centre. However the particles are equally distributed on the surface whereas the square shape has a higher concentration in centre and more around the edges with less equal distribution on the surface

3. Results

Subatomic particle flow distribution is an important factor in designing and manufacturing of nano devices. This is vital where source geometry can make a significant difference in making good use of particle flow. In this research two geometry system is considered square and circular shape. Figure 5 demonstrates the two distributions for a circular and square shape source, the flow in circular geometry is more distributed on the surface whereas the flow in square structure is piled at the corners. Likewise the edges around the square shape caused more concentration in the centre. By taking away the flow in circular form from square shape figure 6 has achieved.

The geometric flow properties of particles, effects their behaviour due to their interactions and their collision dynamics. This could be exhibited by drag force (this is equivalent for electrons), the boundary layers on the surface and wake vortices. Also by long and short range inter-particle forces. Our model tends to have a Normal distribution (Gaussian Distribution) in space. As shown in figure 5 the distribution is balanced in circular shape, where as in square form, particles are mounted around the corners. The Gaussian shape has following property:

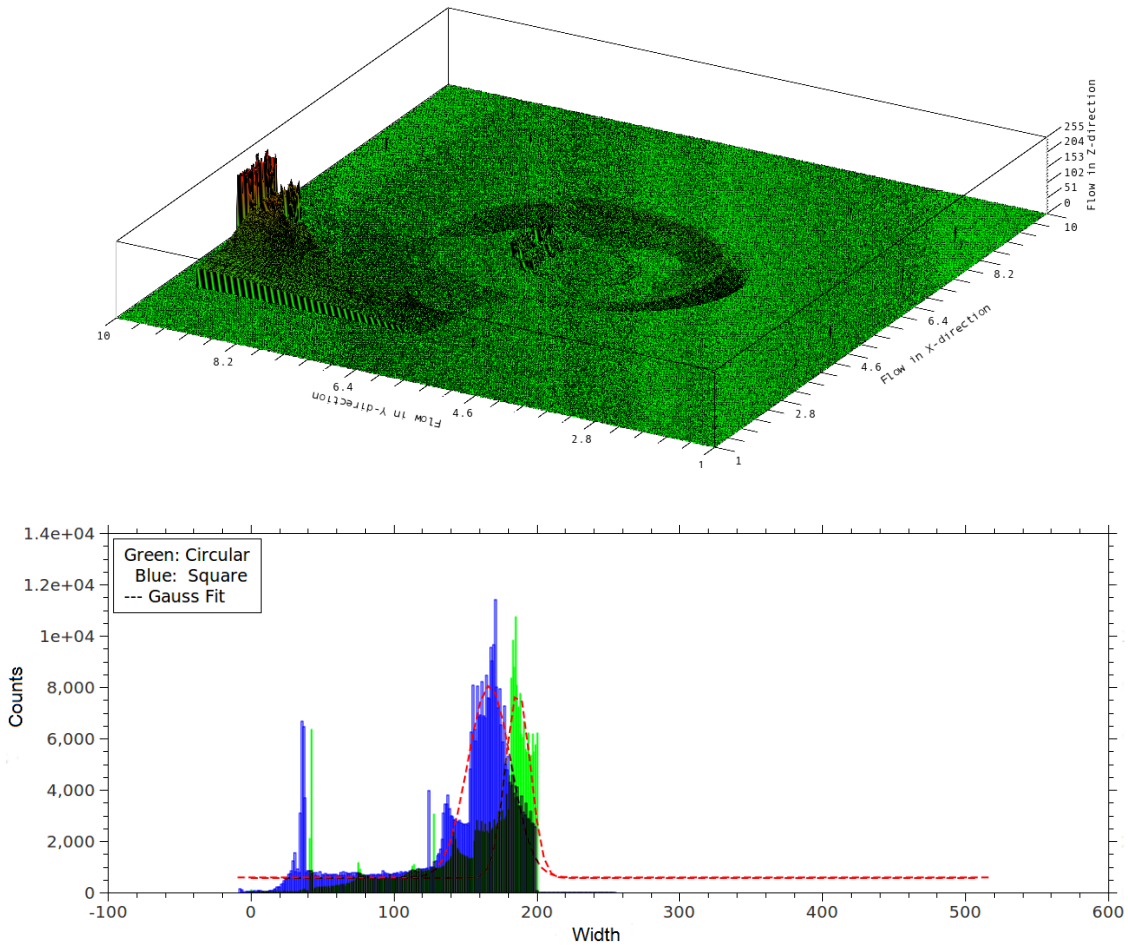

Figure 6. The Particle Distribution in ^{63}Ni. The distribution in circular geometry is lower in centre. However the particles are equally distributed on the surface whereas the square shape has a higher concentration in centre and more around the edges with less equal. The sharp peaks at the centre and the corners are also representing noise in the system.

$$F(x) = y_0 + A\frac{\sqrt{2\pi}}{W}exp(-2(\frac{x - x_c}{W})^2) \tag{25}$$

Here W is the width, x is the length, A is the area and y_0 is the offset. The χ^2/DoF calculated was 9.13(+5). The black area is the area overlapped for both circular and square shape source. As the absorption is concerned, the main processes involves in this model are excitation, ionization. As figure 7 denotes, at energies over 28keV the incident particles start to deposit most of their energies deeper in the film (800 μm thick) with some also penetrating, this means the IMFP is increases. This also corresponds to higher particle range.
The energy loss in 2keV to 28keV range could be in form of heat or bremsstrahlung where the loss is negligible and they deposit almost 99.9% of their initial charge, and 1 % is where the particles break out the film in form radiation. From 28keV to 60keV range a portion of incoming particles escape from the film. However there will be some losses but particles tend to penetrate more into the film before their first collision occurs. Thus Figure 7 presents the fruit of our

calculation and model, it shows the $63Ni$ β^- energy spectrum absorption in 15^P, and the linear line corresponding to full energy deposition (100% efficiency)

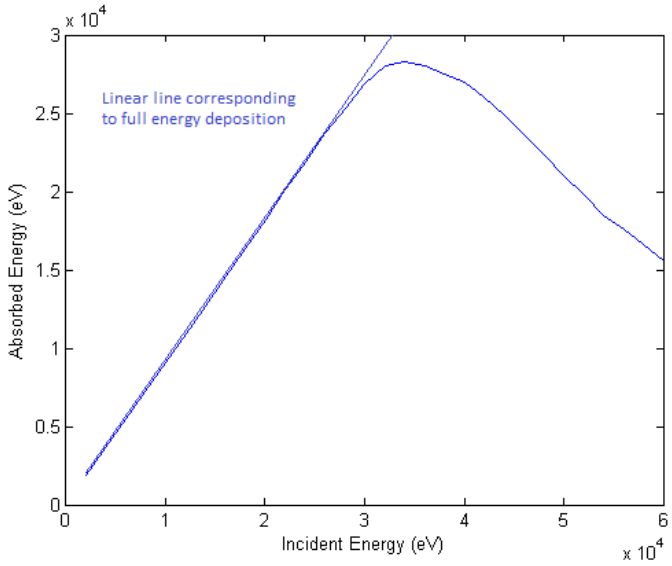

Figure 7. The Energy Absorbed in ^{15}P. The film of ^{15}P is set to have 800 μm. A monoenergetic particle source is created with different energies between $E_{min} = 2keV$ and $E_{max} = 60keV$ to simulate the ^{63}Ni spectrum. As figure denotes, at energies over 28keV the incident particles starts to deposit most of their energies deeper in the film with some also penetrating, this means the IMFP is increases. This also corresponds to higher particle range

Particle range consists of four profiles, longitudinal range, lateral straggling, projected range, and collisional range. The longitudinal range increases because of increase in energy spread(of incoming beam), which is not influenced by dispersion effect. This has a direct relation with beam profile. Although this could be sometimes negligible particularity for a single beam shot but cannot be ignored for a continuous beam (primarily for lower energies). Considering the initial beam profile be ε_z the final Root Mean Square (RMS) is given by [17]:

$$\varepsilon^2_{zfinal} = \varepsilon^2_z + (\frac{17\lambda^2}{40D})^2 \left\langle X'^2 \right\rangle [\left\langle Z^2 \right\rangle + \alpha^2 D^2 \left\langle \delta^2 \right\rangle + 2\alpha D \left\langle Z\delta \right\rangle] \tag{26}$$

Where αD is the longitude dispersion, D is the dispersion factor and X, Z, δ are the angle, position and energy spread respectively. More studies can be done during the experimental prototyping and the effect of beam dispersion could be taken into account before a valid comparison between the final prototype and simulation can be made.
Another dependent of particle range is lateral scattering. As demonstrated in figure 8 beam profile does not significantly change if the distance to any field edges is greater one half of electron ranges [18]. Lateral straggling is significantly affected by size of incoming beam and this is because of correlations between the particle range and its position.
The projected mean range is calculated from CSDA function. The simplified mean free particle range hence is given by [19]:

$$\langle R \rangle = t(1 + t/\lambda_0) \tag{27}$$

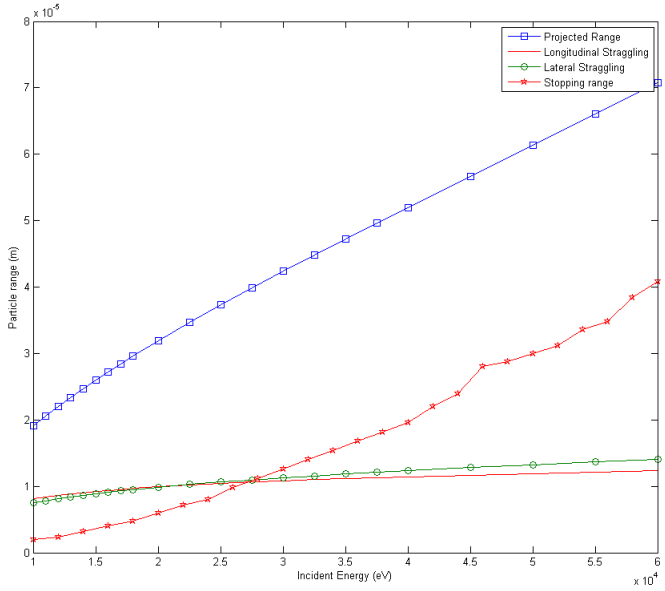

Figure 8. Particle Range Profiles in Phosphorus. The green line demonstrates the Lateral range. Lateral range is largely effected by the beam size, and this is because of particle correlations between range and their positions. The red line shows the longitudinal range. The longitudinal range occurs from beam energy spreading (which is not effected by dispersion). The blue line demonstrates the projected range and can be given using CSDA and finally the red-star line shows the stopping range where the particles deposit most of their energies in the bulk. The red line is the one we are most interested in as a first order approximation

Where λ_0 is mean free path of electrons, and limited to value of thickness (t). When t is approaching R (range), the corresponding value of R can be called L (mean free range), thus L can be recalled as:

$$R = \lambda \frac{[(4L/\lambda) + 1]^2 - 1}{2} \tag{28}$$

Here $\lambda = \lambda_0/4$ and can be given as [20]:

$$\lambda_0 = 2a_0^{-1}(Z)E_0^{\alpha_n(z)} \tag{29}$$

In experimental approximation $\alpha_n(z)$ is the tabulated thickness where $n = 1, 2, ...$ Finally the collisional range is where the incoming beam deposits most of their energy due to the collision. This value represents an accumulated depth in the film where most of the interactions take place. This could later facilitate an understanding of an optimum thickness required for the application.

4. Conclusion

This report has discussed modelling of ^{63}Ni β-source doped in phosphorous (^{15}P). The energy loss processes are discussed and analysed theoretically and experimentally. The Q value calculated for our β^- source (^{63}Ni) was 67keV with mean energy of 17keV. Interactions of β particles with ^{15}P bulk has led to energy loss and charge deposition. Thus to measure the maximum output charge first it is appropriate to look at the number of decays per second. Hence

having ^{63}Ni with half life of 3.1567(+9)s, the probability of decay in one second is 2.196(−10). Also by having mass of ^{63}Ni as 1.044(−22)g the number of atoms in $10mg$ will be 9.57(+19) hence $\bar{n}$ is equal to 2.103(+11) (this values represent the theory, of-course the real application values are much less). The energy loss analysed in this model by implementing discrete points from $^{63}Ni - \beta^-$ spectrum to simulate the interaction of incoming particles. The total energy loss calculated in $800\mu m$ ^{15}P was $5.63(+5)eV.s^{-1}$. However a portion of incoming beams will be lost due to penetration through the film.

5. Acknowledgement

The author is grateful to Dr. T. Leadbeater, Dr. M. Ward, for stimulating discussions. Computations were performed in the Nano Laboratory of the Department of Mechanical engineering and Department of Physics and Astronomy at the University of Birmingham.

References

[1] Franklin P 1958 *An Introduction to Fourier Methods and the Laplace Transformation* (New York: Springer) p 158
[2] Widlund O B 1987 *International Symposium on Domain Decomposition Methods for Partial Differential Equations* 113–128
[3] Babuska I and Gatica G N 2003 *Nubmers and Methods Partial Differential Equations* 192–210
[4] Geiger C and Marsden E 1909 *Proc. R. Soc. Lond* **A82** 495–500
[5] Reimer L K H 2008 *Transmission Electron Microscopy: Physics of Image Formation* (5th edition, Springer)
[6] Wentzel M R and Vos M 2006 *Nucl. Instrum. Methods Phys* **Res. B** 998–1011
[7] Schnatterly S E 1979 *Solid State Physics* **14** 275–358
[8] Ding Z J and Shimzu R 1988 *Surface Science* **197** 539–554
[9] CJ Tung J A and Ritchie R 1979 *Surface Science* **81** 427
[10] Inokuti M 1971 *Rev. Mod. Phys.* **43** 997–347
[11] FBanhart 1999 *Rep.Prog.Phys.* **62** 1181
[12] Pines D and Nozieres P 1966 *Rep.Prog.Phys.* **1**
[13] Ganachaud J and Cailler M 1979 *Surface Sci.* **83** 498
[14] A Desalvo A P and Rosa P 1984 *J. Phys.* **D17** 2455
[15] Penn D R 1978 *Physical Review B* **35** 483–486
[16] S Tanuma C J P and Penn D R 1991 *Surf. and Interface Anal.* **17** 927
[17] J Thangaraj J Ruan A S J R T K A H L J S Y E S T M H E 2012 *IEEE, Proceedings of IPAC2012* 49–51
[18] ICRU 1972 *International Commission on Radiation Units and Measurements Report* **21**
[19] Rose M E 1940 *Phys. Rev.* **58**(1) 90–90
[20] Tabata T 1968 *Journal of Applied Physics* **39** 5342–5343